Thermal Stress Analysis of Residual Stress in a Cylindrical Aluminum Casting with Cast-in GCI Liner, Taking Recovery Behavior Effect into Account

YUICHI MOTOYAMA, NAOYUKI EBIHARA, HIDETOSHI SHIGA, TAKESHI SATO, HIROSHI KAMBE, and MAKOTO YOSHIDA

Most aluminum cylinder blocks produced using high-pressure or low-pressure die-casting processes require gray cast iron liners (GCI liners) to compensate for their insufficient wear resistance and heat resistance of the Al-Si-Cu alloys. However, the cast-in liners cause excessive residual stress at the cylinder bore region. The resultant residual stress induces distortion of the cylinder liner. These inconveniences hinder development of more efficient engines. Therefore, an accurate thermal stress analysis technique has been sought to predict the residual stress and distortion of the cylinder liner. For accurate thermal stress analysis, we have already developed an elastoplastic-creep constitutive equation for which the inelastic strain developed at high temperatures does not contribute to strain hardening that occurs at low temperatures by duplicating the recovery behavior. Our earlier investigation using this equation has already revealed that incorporation of the recovery in the alloy constitutive equation is effective for improving the prediction accuracy of the thermal stress developed during casting. However, this conclusion was obtained only for a simple shape casting with a uniaxial thermal stress state. Effects of the developed constitutive equation have not been discussed for a casting closer to an actual cylinder block. For this study, a cylindrical aluminum casting with GCI (ISO 300) insert was produced. Then, the circumferential strain of the GCI liner was measured *in-situ* during casting. Measurements were taken of the residual stresses of the cylindrical aluminum casting and GCI liner, and of the liner deformation at a room temperature. The experimentally obtained results supported a discussion of the predictive accuracies of the elastoplastic-creep constitutive equation and the classical elastoplastic constitutive equation. A comparison revealed that the elastoplastic-creep constitutive equation for the aluminum casting has better predictive accuracy than the classical elastoplastic equation for residual stress, liner deformation, and the circumferential strain of a GCI liner during casting. Investigation of the simulated strain components of the cylindrical aluminum casting during casting indicated incorporation of the recovery in the alloy constitutive equation as a main factor improving the predictive accuracy.

YUICHI MOTOYAMA is with the Advanced Manufacturing Research Institute, National Institute of Advanced Industrial Science and Technology, 1-2-1, Namiki, Tsukuba, Ibaraki, 305-8564, Japan. Contact e-mail: y.motoyama@aist.go.jp NAOYUKI EBIHARA is with the Department of Modern Mechanical Engineering, Waseda University, 3-4-1 Ookubo, Shinjuku-ku, Tokyo, 169-0072, Japan. HIDETOSHI SHIGA, TAKESHI SATO, and HIROSHI KAMBE are with the Nissan Motor Co. Ltd., 6-1, Daikokucho, Tsurumi-ku, Yokohama-shi, Kanagawa, 230-0053, Japan. MAKOTO YOSHIDA is with the Kagami Memorial Research Institute for Material Science and Technology, Waseda University, 2-8-26, Nishiwaseda, Shinjuku-ku, Tokyo, 169-0051, Japan.

I. INTRODUCTION

MOST cylinder blocks intended for automotive use are made from Al-Si-Cu alloys with gray cast iron (GCI) liners cast into the cylinder bores to improve wear resistance and heat resistance. The bore regions of an aluminum cylinder block are prone to undergo circumferential tensile residual stress during casting because of the different coefficients of thermal expansion (CTEs) of the aluminum alloy ($2.6 \times 10^{-5} \text{ K}^{-1}$) and GCI ($1.4 \times 10^{-5} \text{ K}^{-1}$) (Carrera *et. al.*[1]). Lombardi *et al.*[2] reported that a cylinder bore with residual stress causes the dimensional distortion of the cylinder bore during service operation. That distortion greatly reduces engine operating efficiency because of compression loss in the combustion chamber. They made the cylinder block

with GCI liners using 319 type alloys. The residual stress distribution was measured at its cylinder bridge area using the neutron diffraction following thermal sand reclamation (TSR), T7 heat treatment, and service testing of the casting. The average magnitudes of the tensile residual stress of the hoop, radial, and axial directions were, respectively, 180, 100, and 160 MPa at the cylinder bridge in the TSR condition. They also investigated[3] T4 heat-treatment effects on the residual stress of the aluminum cylinder block in the TSR condition. They reported that the solution heat treatment in T4 heat treatment completely relieved residual stress. The subsequent air cooling led to the development of tensile stress at the top of the cylinder. Ahmad et al.[4] measured the residual stress of a T5 aluminum cylinder block with GCI liners. Results showed that the hoop tensile stress was 300 MPa and that the T5 treatment did not relieve residual stress effectively. Therefore, prediction of the residual in the as-cast condition is important for T5 heat treatment.

This study was conducted to obtain knowledge for accurate prediction of residual stress and liner deformation in as-cast aluminum cylinder blocks produced using the high-pressure die-cast processing. Accurate predictions of the residual stress and liner deformation are required for the development of the efficient automobile engines because aluminum cylinder blocks with GCI liners produced using high-pressure die-cast processing are usually used in the as-cast state.

The choice of the alloy constitutive equation used for the thermal stress analysis is well known to affect the predictive accuracy of thermal stress analysis strongly. Hofer et al.[5] simulated the residual stress of aluminum high-pressure die castings using an elastoplastic constitutive equation. Then, they assessed the accuracy of the residual stress prediction by comparing simulation results with the residual stress measurements. However, the simple elastoplastic constitutive equation is unable to duplicate typical metallurgical phenomena occurring at high temperatures, such as the strain-rate dependence of the stress–strain curve and the recovery behavior described below. Motoyama et al.[6] developed an elastoplastic-creep constitutive equation for the Al-Si-Cu die-cast alloy (Japan patent, patent number: JP6268584). Using the developed equation, they[7] also compared the thermal stress analysis results with in-situ measurements of the axial thermal stress of a simple I-shaped Al-Si-Cu casting during casting. Results of the comparison revealed that the alloy constitutive equation required consideration of the strain-rate dependence of the stress–strain curves (strain-rate dependence) and recovery behavior for the accurate prediction of the thermal stress of the I-shaped casting during casting. In their study, recovery meant a metallurgical phenomenon by which the inelastic strain developed at high temperatures does not contribute to strain-hardening behavior at low temperatures (hereinafter, recovery) because recovery and recrystallization at high temperatures annihilate the dislocation and reduce the dislocation density increased by the plastic deformation. Therefore, we checked alloy constitutive equations used in earlier studies to ascertain whether the strain-rate dependence and recovery were incorporated, or not. This study reviews earlier studies that conducted thermal stress analysis during the casting of aluminum cylinder blocks with GCI liners or castings, which are analogous to cylinder blocks with GCI liners. Via thermal stress analysis with an elastoplastic constitutive equation,
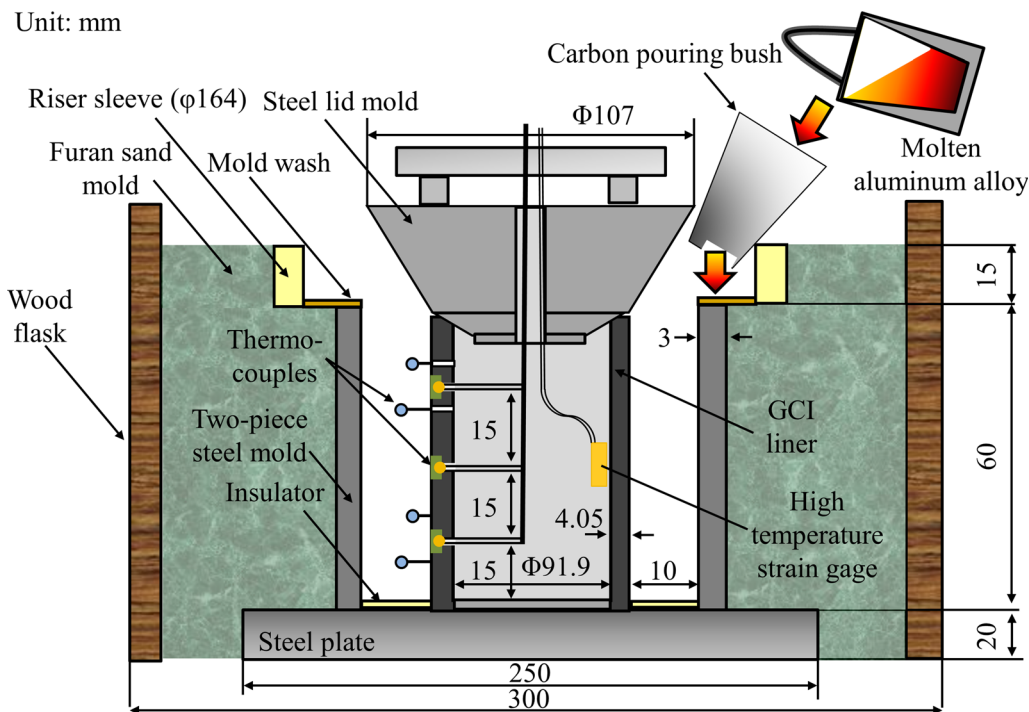

Fig. 1—Schematic illustration of the casting mold used for cylindrical casting with a cast-in GCI liner.

Dong et al.[8] predicted cold cracking of a casting with cast-in steel lings. However, they did not describe consideration of the recovery and the strain-rate dependence in the alloy constitutive equation. The classical elastoplastic constitutive equation is generally unable to duplicate both the strain-rate dependence and recovery. Using MAGMA software, Wasmuth et al.[9] and Čech et al.,[10] respectively, simulated the residual stress of a cylindrical aluminum casting with the cast-in steel liner and an aluminum die-casting cylinder block with GCI liners. Nevertheless, neither study explained what constitutive equations were used for their thermal stress analyses. From the review described above, one finds that further investigation must be undertaken to assess the effects of strain-rate dependence and recovery in the alloy constitutive equation to raise the predictive accuracy of thermal stress analyses of cylinder blocks with GCI liners. For investigating these points, this study produced a cylindrical aluminum casting with a GCI liner. When making its casting, this study obtained measurements not only of the residual stresses of the aluminum casting and the GCI liner; we also took *in-situ* measurement of the compressive strain developed in the GCI liner during casting. In addition to these measurements, the GCI liner distortion was measured. Regarding the thermal stress analysis, this study adopted the classical elastoplastic constitutive equation and our already developed elastoplastic-creep constitutive equation, which was able to duplicate both the strain-rate dependence and recovery. By comparing the results obtained using two equations with the experimental results, this study elucidates effects of considering the recovery behavior in the alloy constitutive equation in the thermal stress analysis of the cylindrical aluminum casting with the cast-in GCI liner.

II. EXPERIMENTAL PROCEDURES

Figure 1 presents a schematic illustration of the experimental apparatus used for this study. After concentric grooves were cut in the upper surface of the steel plate, a GCI cylinder liner and cylindrical steel molds with a vertical split were installed on the grooves. By installing the liner and molds on the grooves, the cylinder liner and aluminum casting positions were precisely concentric during casting. The space between the wood flask and steel molds was filled with furan sand as the back-up sand. A circle insulator was installed on the steel plate to prevent cooling of the casting through the steel plate and to cool the aluminum casting uniformly in the circumference direction to the greatest degree possible during casting. Uniform cooling of the aluminum casting produces the uniform tightening of the aluminum casting for the GCI liner during casting. A circular riser sleeve was installed at the top to make a riser. A steel lid was installed on the GCI liner to prevent the melting alloy from infiltrating inside the liner. The lid had a center hole through which lead wires of thermocouples and a high-temperature strain gage came out. They were connected to a measurement logger.

To measure the temperature histories of the aluminum casting with sheath thermocouples during casting, through-holes of 1.2 mm diameter were drilled into the liner at the point shown in Figure 2. Sheath K-type thermocouples of 1 mm diameter were taken out of the holes. The gaps between the hole and the thermocouple were filled with a ceramic bond to fix the thermocouple at the position and to prevent the molten alloy from entering the liner through the gap. To measure the liner temperature with the thermocouple elements,
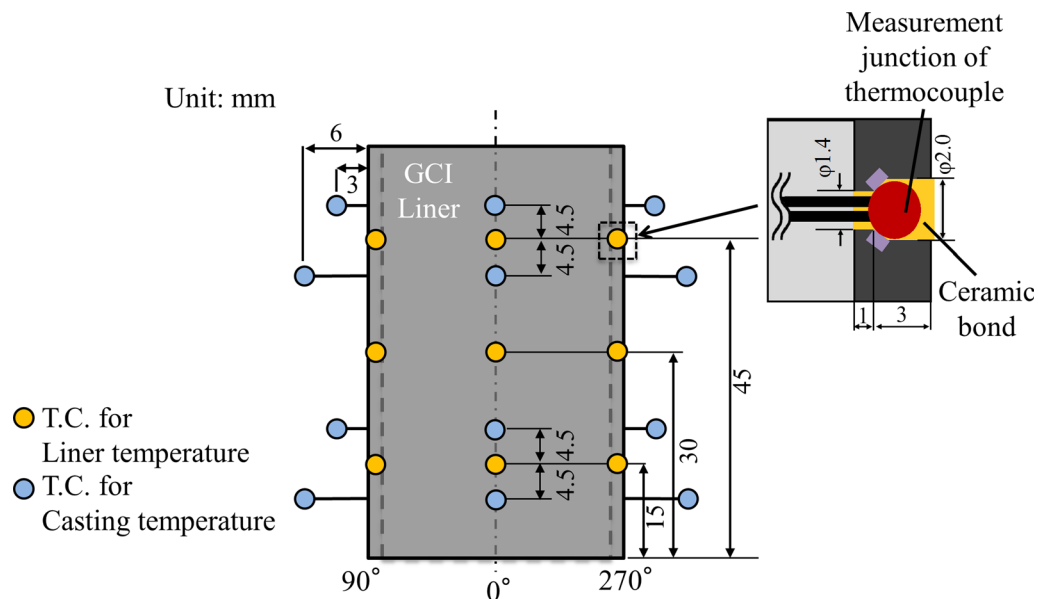

Fig. 2—Thermocouple locations for measuring the GCI liner and casting temperatures.

through-holes of 1.4 mm diameter were drilled into the liner at the position shown in Figure 2.

In addition, at the same positions, 2.0-mm-diameter holes were drilled at 3 mm from the liner surface to make fixation points for the thermocouples. The measurement junctions of the thermocouples were hooked on the fixation points. Gaps between the measurement junction and the fixation point were filled with the ceramic bond, as shown in Figure 2. Thermocouples were installed for the experiments to obtain the temperature histories used in thermal analysis and for the *in-situ* strain measurement of the GCI liner. The thermocouples were not installed for measurements to obtain the residual stress and deformation because the reproducibility of the temperature histories of the casting and liner had already been confirmed from the temperature measurements described above.

A high-temperature strain gage was welded at point (1) in Figure 3 in the circumferential direction at the center position of the GCI liner in the height direction to measure the circumferential thermal strain of GCI liner during casting. The CTEs between the high-temperature strain gage welded to the liner and the GCI liner differ because the strain gage is made from Inconel 600. Therefore, the high-temperature strain gage welded to the liner sensed the apparent strain deriving from the difference of CTEs in addition to the compressive strain caused by tightening of the aluminum casting. To remove the apparent strain component from the strain measured by the high-temperature strain gage, this study conducted a preliminary experiment in which the GCI liner with the high-temperature strain gage was heated from RT to 723 K (500 °C). Thereby, this study obtained only the apparent thermal strain with temperature. By subtracting the apparent thermal strain component from the measured strain at each temperature, this study obtained the circumferential compressive strain attributable only to the tightening of the aluminum casting with temperature during casting. Table I(a) presents the chemical composition of Al-Si-Cu die casting alloy (JIS ADC12 (AISI 383.0)) used for this study. The alloy was poured at 953 K (680 °C). The pouring time, approximately 2.3 seconds, was observed from a movie of the pouring.

Figure 4 shows the cylindrical aluminum casting with the GCI liner for experiments. After the casting cooled to the RT, the steel lid was removed from the casting. The strain gages were attached to the aluminum casting and GCI liner in the circumferential direction at points (1), (2), (3), and (4) in Figure 3. Then, the aluminum casting was cut with a band saw. The residual elastic strains of the casting and the liner were released. The residual stresses were ascertained by multiplying the released elastic strain by Young's modulus of RT. Young's moduli of the ADC12 and GCI used were, respectively, 77.4 and 138.5 GPa. These values were quoted from measurements of the resonance method described later. To evaluate the GCI liner deformation, the liner diameter before and after casting was measured at 30 mm height from the bottom at RT using a three-dimensional measuring device.

III. ANALYTICAL CONDITIONS

A. *Thermal and Fluid Flow Analysis Conditions*

This study used CAPCAST 3.5.7 for thermal and fluid flow analyses. This software is a finite-element software package developed by EKK inc.

Figure 5 shows the CAD model used for analyses. The thermal and fluid flow analyses were conducted on a
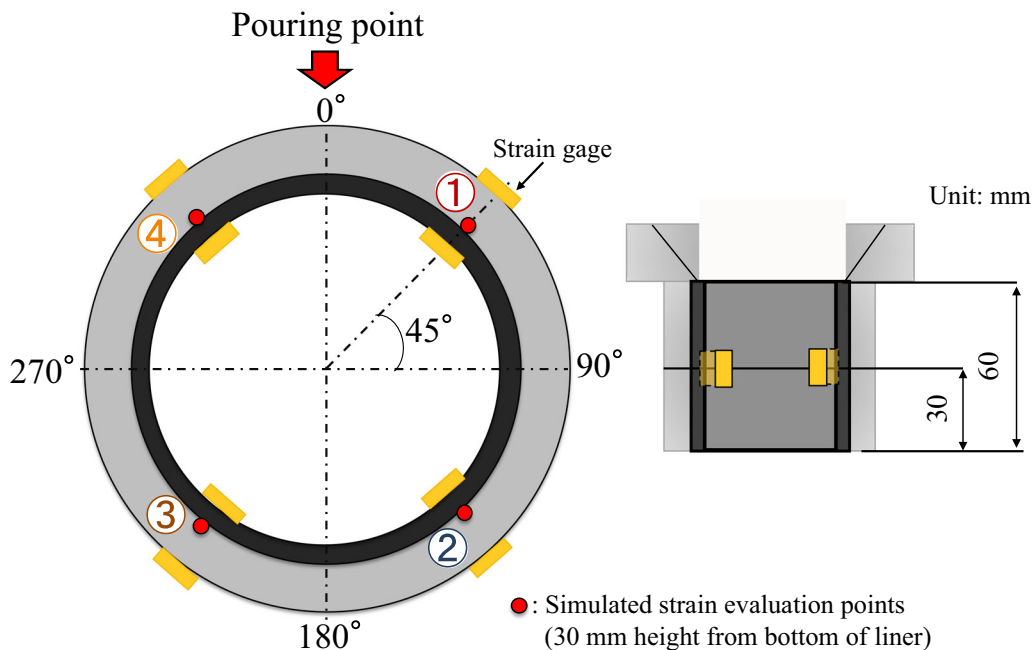

Fig. 3—Casting and GCI liner points where strain gages were attached to measure residual stress at RT.

Table I. Chemical Compositions of (a) JIS ADC12 Alloy (AISI 383.0) and (b) Gray Cast Iron

(a) Si	Fe	Cu	Mn	Mg	Zn	Ni	Wt Pct Al
10.7	0.93	2.5	0.08	0.16	0.15	0.03	bal.

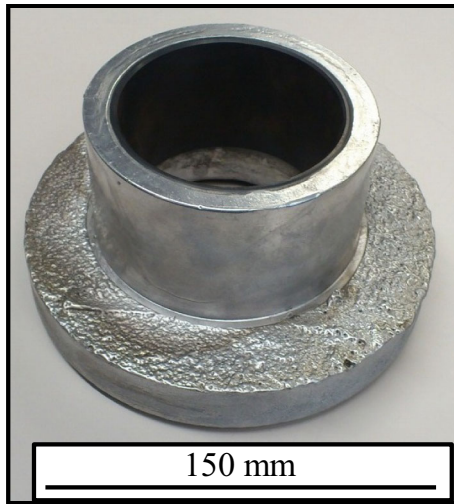| (b) C	Si	Mn	Cr	P	S	Wt Pct Cu
3.16 to 3.28	2.11 to 2.40	0.60 to 0.65	0.146 to 0.147	0.14	0.073 to 0.076	0.25

Fig. 4—Cylindrical aluminum casting with cast-in GCI liner.

1/2 model because the casting and the molds were symmetrical. Thermal properties used in the analysis are presented in Table II, and Figures 6(a) and (b).

The thermophysical properties of ADC12 and the gray cast iron were obtained using thermodynamics software (JMat Pro; Sente Software Ltd.). The obtained solidus and liquidus temperatures of ADC12 were, respectively, 763 K (490 °C) and 850 K (577 °C). General data were used for the other materials. When an inaccurate thermal analysis result of the casting is used for the temperature history of casting in thermal stress analysis, the thermal stress analysis cannot predict the thermal stress of the casting with high accuracy. In such cases, it is difficult to discuss the predictive accuracy of the thermal stress analyses by comparing the analyses with experiments. Therefore, in this study, high reproducibility of the casting temperature was achieved by optimizing the heat transfer coefficient between the casting and the metal molds using trial-and-error method whereby its heat transfer coefficient was changed until satisfactory agreement was achieved between the simulated and experimental temperatures of the casting and the molds. Table III shows the heat transfer coefficients found through trial-and-error method, along with the initial conditions used for thermal analyses.

B. Thermal Stress Analysis

1. Analysis conditions

Commercial finite-element software ABAQUS was used for the thermal stress analyses. The aluminum casting and liner were modeled using eight-node brick elements. The temperature histories of the casting and the liner were imported from the thermal analysis results.

As shown in Figure 7, the GCI liner was modeled using the elastoplastic constitutive equation. The steel lid was modeled as a rigid body in the thermal stress analysis. This study applied two constitutive equations to ascertain the recovery effects on the predictive accuracy of the thermal stress analysis for the aluminum casting. One was a classical elastoplastic equation that was unable to duplicate the recovery and the strain-rate dependence. The other was our previously developed elastoplastic-creep equation, which was able to duplicate both the recovery and the strain-rate dependence. The constraint conditions shown in Figure 7 prevented the analytical model from inducing rotation and translation motions without constraining the thermal contraction of the aluminum casting in the analysis. Because the outer surface of the actual GCI liner had a spiral groove, the aluminum casting and liner are expected to be in close contact during experiments. Therefore, a friction coefficient of 0.15 was assigned between the liner and aluminum casting for analyses. The following two steps were adopted to obtain the circumferential residual stresses of casting and liner in these analyses. First, similar to the experiment, the steel lid was removed from the model after cooling to RT, and this state was the reference state for the residual stress calculation. Second, the aluminum casting was cut. Thereby, the residual stress was released. The residual stresses of the liner and casting were found by calculating the stress changes from the reference state to that after cutting.

2. Constitutive equation used for the thermal stress analysis

The following equations were used as the elastoplastic equation for ADC12:

$$\varepsilon_{ij} = \varepsilon_{ij}^{e} + \varepsilon_{ij}^{p} + \varepsilon_{ij}^{th} \qquad [1]$$

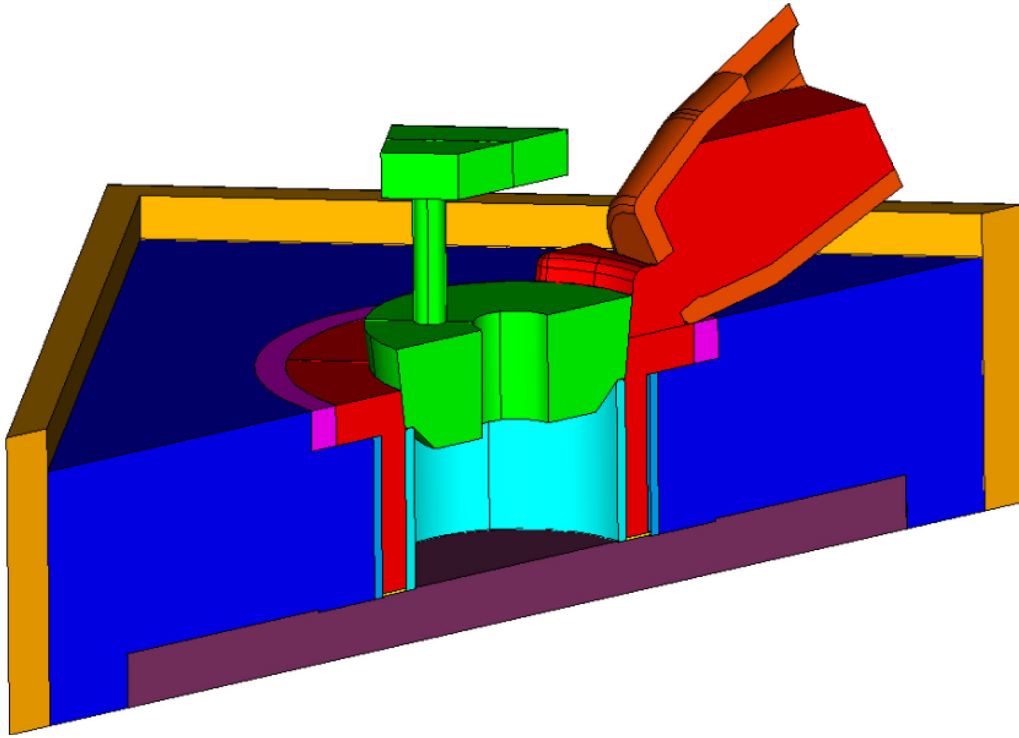$$\sigma_{ij} = D_{ijkl}(T)\varepsilon_{kl}^{e} \qquad [2]$$

Fig. 5—½ CAD model for thermal analysis during casting.

$$f(\sigma_{ij}, T) = \sqrt{3J_2} - \sigma_y(T) - K \qquad [3]$$

$$K = K(\varepsilon_{eff.}^p, T) \qquad [4]$$

$$\varepsilon_{ij}^p = \lambda \frac{\partial f}{\partial \sigma_{ij}} \qquad [5]$$

$$\dot{\varepsilon}_{ij} = \dot{\varepsilon}_{ij}^e + \dot{\varepsilon}_{ij}^p + \dot{\varepsilon}_{ij}^c + \dot{\varepsilon}_{ij}^{th} \qquad [6]$$

$$\dot{\sigma}_{ij} = D_{ijkl}(T)\dot{\varepsilon}_{kl} \qquad [7]$$

$$\dot{\varepsilon}_c = A(T)\sigma^{n(T)} \qquad [8]$$

In the above equations, T stands for the temperature, σ_{ij} denotes the stress, ε_{ij}^e signifies the elastic strain, ε_{ij}^p represents the plastic strain, ε_{ij}^{th} is the thermal strain, D_{ijkl} is the elastic coefficient tensor, J_2 is the second invariant of the deviatoric stress tensor, and $\sigma_y(T)$ represents the initial yield stress dependent on the temperature. In addition, $\varepsilon_{eff.}^p$ stands for the equivalent plastic strain, λ denotes a positive scalar, and K is the hardening parameter, which is a function of the temperature and equivalent plastic strain. Data of stress–inelastic strain relations were inputted in tabular form for each temperature.

The following equations constitute the elastoplastic-creep equation used for ADC12. As with the elastoplastic equation described above, the plastic term in the elastoplastic-creep equation adopted the von Mises yield function, the isotropic hardening law, and the associated flow rule. The Norton law was used as the creep term. $A(T)$ and $n(T)$ are material parameters. Also, $\dot{\varepsilon}_{ij}^c$ is the creep strain rate.

The characteristics of this elastoplastic-creep equation constructed for ADC12 are as follows. This equation is able to duplicate the strain-rate dependence of the stress–strain curves at temperatures higher than 573 K (300 °C) by introducing the creep term. Moreover, at these temperatures, the stress–inelastic strain curve has the large part of the steady flow stress (steady-state) region, following the small part of the strain-hardening region. An assumption of the elastoplastic-creep equation is that the inelastic strain developed at the steady-state region does not contribute to strain hardening at low-temperature range. Its region can be represented using the steady-state creep law (Eq. [8]). This assumption is reasonable because the strain hardening and softening attributable to the dynamic recovery are balanced in its region. The plastic constitutive equation was adopted to represent only the initial strain-hardening region. As a result, almost none of the inelastic strains developed at high temperatures increases the strain-hardening parameter (Eq. [4]) and does not contribute to strain hardening (increase of the initial yield stress) at RT. Consequently, this equation is

Table II. Thermal Properties Used in the Thermal Analysis

	Thermal Conductivity		Specific Heat		Density		Latent Heat
	T, K (°C)	λ (W m^{-1} K^{-1})	T, K (°C)	C_p (J/kg K)	ρ (kg m^{-3})		L (J/kg)
ADC12	473 (200)	152.7	673 (400)	1029	Liquid	2540	709527
	763 (490)	142.9	753 (480)	1065.3	Solid	2610	—
	813 (540)	131	886.8 (613.8)	1092.8	—	—	—
	823 (550)	125.3	968 (695)	1114.1	—	—	—
	828 (555)	120.6	—	—	—	—	—
	833 (560)	113.1	—	—	—	—	—
	838.5 (565.5)	100.1	—	—	—	—	—
	841.5 (568.8)	81.5	—	—	—	—	—
	850.5 (577.5)	77.6	—	—	—	—	—
	973 (700)	81.5	—	—	—	—	—
Gray cast iron	373 (100)	30.5	373 (100)	522.6	—	7200	—
	473 (200)	31.1	473 (200)	554.8	—	—	—
	573 (300)	31.4	573 (300)	592.2	—	—	—
	623 (350)	31.4	623 (350)	614.1	—	—	—
	673 (400)	31.2	673 (400)	638.9	—	—	—
	723 (450)	30.9	723 (450)	667.4	—	—	—
	773 (500)	30.5	773 (500)	700.9	—	—	—
	823 (550)	30	823 (550)	739.8	—	—	—
	873 (600)	29.4	873 (600)	833.7	—	—	—
	923 (650)	28.8	923 (650)	895.5	—	—	—
Steel mold and plate	373 (100)	51.1	373 (100)	449.9	—	7840	—
	573 (300)	44.4	773 (500)	539.9	—	—	—
	673 (400)	42.6	1273 (1000)	669.9	—	—	—
	973 (700)	31.8	—	—	—	—	—
Sand mold	373 (100)	0.42	373 (100)	954.8	—	1413	—
	473 (200)	0.44	473 (200)	978.4	—	—	—
	573 (300)	0.46	573 (300)	1001.3	—	—	—
	673 (400)	0.46	673 (400)	1023.2	—	—	—
	773 (500)	0.45	773 (500)	1044.2	—	—	—
	873 (600)	0.45	873 (600)	1066.1	—	—	—
	973 (700)	0.45	973 (700)	1088.1	—	—	—
	1073 (800)	0.46	1073 (800)	1109.8	—	—	—
Wood flask	—	79.1	—	1469.3	—	1902	—
Insulator	—	0.084	—	1000.5	—	150	—

able to represent the recovery. Below 573 K (300 °C), the elastoplastic-creep equation changes to an almost elastoplastic equation by decreasing the value of the creep parameter "A" to almost 0. Our previous study already elucidated details of the characteristics described above.[6]

Gray cast iron shows very different strengths in tension and compression. Its compressive yield stress is more than three times higher than the tensile yield stress. To duplicate these mechanical behaviors of the gray cast iron, this study used the following cast iron plasticity model, which was already included in the Abaqus software.[11]

$$\varepsilon_{ij} = \varepsilon_{ij}^\mathrm{e} + \varepsilon_{ij}^\mathrm{p} + \varepsilon_{ij}^\mathrm{th} \quad [9]$$

$$\sigma_{ij} = D_{ijkl}(T)\varepsilon_{kl}^\mathrm{e} \quad [10]$$

$$\cos(3\theta) = \frac{J_3}{2}\left(\frac{3}{J_2}\right)^{3/2} \quad [11]$$

$$F_\mathrm{t} = \frac{2}{3}\cos(3\theta)\cdot\sqrt{3J_2} - \frac{1}{3}I_1 - \sigma_\mathrm{t}\left(\bar{\varepsilon}_\mathrm{t}^\mathrm{pl}, T\right) = 0 \quad [12]$$

$$F_\mathrm{c} = \sqrt{3J_2} - \sigma_\mathrm{c}\left(\bar{\varepsilon}_\mathrm{c}^\mathrm{pl}, T\right) = 0 \quad [13]$$

In these equations, θ denotes the Lode angel, T denotes the temperature, $\bar{\varepsilon}_\mathrm{t}^\mathrm{pl}$ is the tensile equivalent plastic strain, $\bar{\varepsilon}_\mathrm{c}^\mathrm{pl}$ is the compressive equivalent plastic strain, $\sigma_\mathrm{t}\left(\bar{\varepsilon}_\mathrm{t}^\mathrm{pl}, T\right)$ is the tensile yield stress, $\sigma_\mathrm{c}\left(\bar{\varepsilon}_\mathrm{c}^\mathrm{pl}, T\right)$ represents the compressive yield stress, F_t stands for the
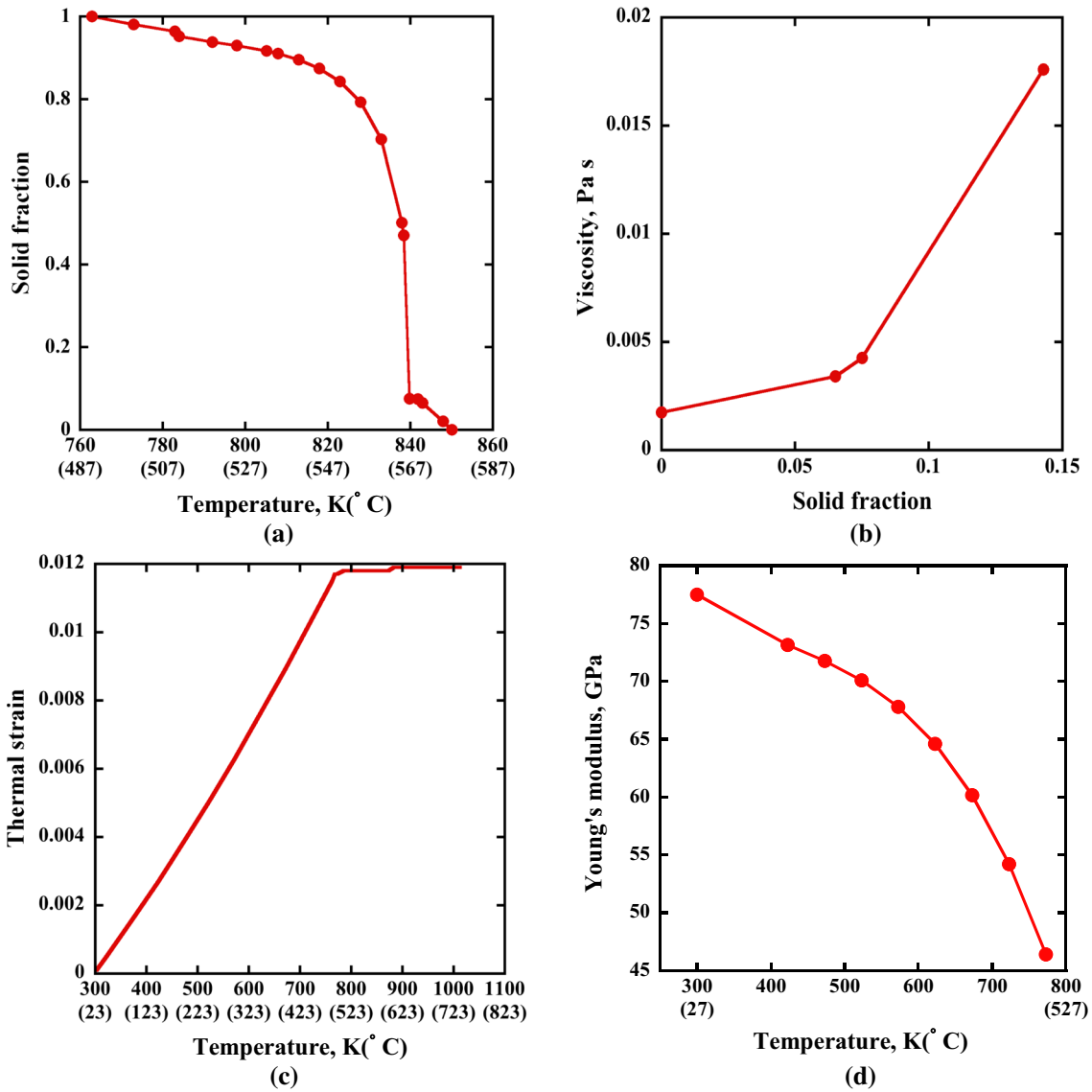
Fig. 6—Thermophysical properties of ADC12 used in thermal and fluid flow and thermal stress analyses: (a) solid fraction, (b) viscosity, (c) thermal strain, and (d) Young's modulus.[6]

yielding surface in tension, and F_c signifies the yielding surface in the compressive stress region. Also, J_3 represents the third invariant of the deviatoric stress. I_1 denotes the first invariant of the stress. The tensile and the compressive equivalent plastic strains are expressed as presented below:

$$\dot{\varepsilon}_{vol}^{pl} = \dot{\varepsilon}_{ij}^{pl} : I \qquad [14]$$

$$\dot{e}^{pl} = \frac{2}{3}\dot{\varepsilon}_{ij}^{pl} : \left(\frac{3}{2q}\right)S_{ij} \qquad [15]$$

$$\bar{\varepsilon}_{c}^{pl} = \dot{e}^{pl} \qquad [16]$$

$$\bar{\varepsilon}_{t}^{pl} = \frac{1}{\sigma_t}\left(-\frac{I_1}{3}\dot{\varepsilon}_{vol}^{pl} + \sqrt{3J_2}\dot{e}^{pl}\right). \qquad [17]$$

where $\dot{\varepsilon}_{vol}^{pl}$ and $\dot{e}^{pl}$ denote the volumetric and deviatoric components of the plastic strain, respectively. q is the Mises equivalent stress. S_{ij} denotes the deviatoric stress. I is the second-order unit tensor.

The flow rule is expressed as shown below:

$$\gamma\dot{\varepsilon}_{ij}^{pl} = \dot{\lambda}\frac{\partial G}{\partial \sigma_{ij}} \qquad [18]$$

$$\frac{(I_1/3 - G_t)^2}{a^2} + 3J_2 = 9G_t \quad \left(p < \frac{\sigma_e}{3}\right) \qquad [19]$$

Table III. Initial and Boundary Conditions Used in the Thermal Analysis

Initial Conditions	
Pouring temperature	953 K (680 °C)
Initial temperatures of liner, steel molds, plate, sand mold, flask, and insulators	290 K (17 °C)
Pouring time	2.3 s

Boundary Conditions	Heat Transfer Coefficient, W m^{-2} K^{-1}
Casting/liner	2100
Casting/steel mold (pouring side)	2100
Casting/steel mold (opposite pouring side)	4200
Casting/steel mold (right and left sides)	2100
Casting/air	50
Casting/insulator	4.2
Liner/steel mold	4200
Liner/air	42
Steel mold/sand mold	2100
Sand mold/wood flask	4200
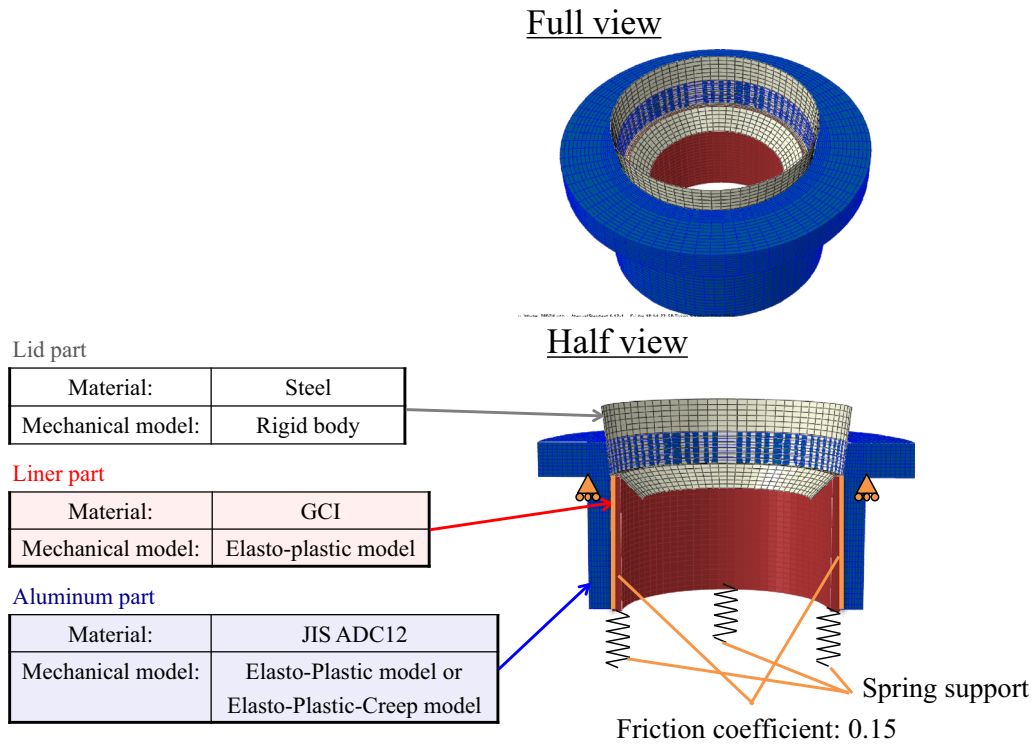
Fig. 7—FE model, constitutive equations for each part, and applied mechanical boundary conditions for thermal stress analysis.

$$\sqrt{3J_2} = 3G_c \quad \left(P \geq \frac{\sigma_c}{3}\right) \qquad [20]$$

In the above equations, γ is a material parameter that controls plastic dilatation; it is a function of the plastic Poisson's ratio v_{pl}. The default value of 0.04 was used for v_{pl} in this study. $\dot{\lambda}$ is the plastic multiplier. G is the potential that can take one of two values, G_t and G_c. G consists of the Mises cylinder in compression with an ellipsoidal cap in tension. Then, the ellipse shape is controlled by a, which is chosen such that it passes through the two points $(-\gamma\sigma_t/3, \gamma\sigma_t)$ and $(\sigma_c/3, \sigma_c)$.

3. *Mechanical properties of ADC12 for constitutive equations*

Our earlier study measured Young's moduli of ADC12 by the resonance method and its tensile stress–strain curves.[6] This study also used these values. Young's moduli were inputted at RT and at temperatures of 423 K to 773 K (150 °C to 500 °C) with 50 K steps, as shown in Figure 6(d). Using the Young's

moduli, stress–inelastic strain curves were obtained by subtracting the elastic strain component from the true stress–true strain curves at respective temperatures. The stress–inelastic strain curves of ADC12 were used to ascertain the material constants of the constitutive equations and for inputting the data into the equations. The temperature dependent CTEs of the alloys were obtained using JMatPro.[12] It was assumed for this study that the liquid was free to move at temperatures higher than the solidus temperature. We neglected the thermal contraction of the alloy at temperatures higher than the solidus temperature of 763 K (490 °C). The obtained CTE data were adjusted to duplicate the behavior described above. The resultant thermal strain curve of ADC12 for the thermal stress analysis is shown in Figure 6(c). The tensile stress–strain curve of RT was stretched at 0.001 s^{-1}. Stress–strain curves from 423 K (150 °C) to 723 K (450 °C) with 50 K steps were obtained at strain rates of 0.001 and 0.0001 s^{-1}. These curves were obtained using a cooling test in which the tensile specimens received solution heat treatment before cooling to each tensile testing temperature. The cooling test is intended to annihilate precipitation in the specimen and to obtain equivalent mechanical properties to those in the as-cast condition to the greatest extent possible. The stress–strain curves above the temperature of 773 K (500 °C), which was higher than the solidus temperature of the alloy, were referred from an earlier report of a study that conducted tensile tests during alloy solidification.[13] For the elastoplastic constitutive equation, data of stress–inelastic strain relations at a strain rate of 0.001 s^{-1} were inputted in tabular form for respective temperatures. The elasto-plastic-creep constitutive equation used the same Young's moduli and CTE of ADC12 as those of the elastoplastic equation presented above. The stress–inelastic strain curves stretched at 0.001 and 0.0001 s^{-1} were used to ascertain the material constants of the creep term and for inputting the stress–plastic strain relations to the plastic term. The stress–plastic

strain curves and the creep constants inputted for the elastoplastic-creep equation used in this study are portrayed in Figures 8 and 9. Figure 10 presents a comparison of the measured and predicted stress–strain responses of ADC12 at strain rates of 0.001 and 0.0001 s^{-1}. Details related to determination of the material constants are represented in a report of our earlier work.[6]

4. *Mechanical properties of GCI for cast iron plasticity*

Tensile and compressive stress–strain curves were obtained using tensile and compressive tests to input the stress–inelastic strain relations in the cast iron plasticity. Tests were conducted from RT to 873 K (600 °C) which the GCI liner experienced during the casting experiment. Blocks of gray cast iron (ISO 300) were produced by pouring the melt into the furan sand mold. Table I(b) presents its chemical composition. The blocks were
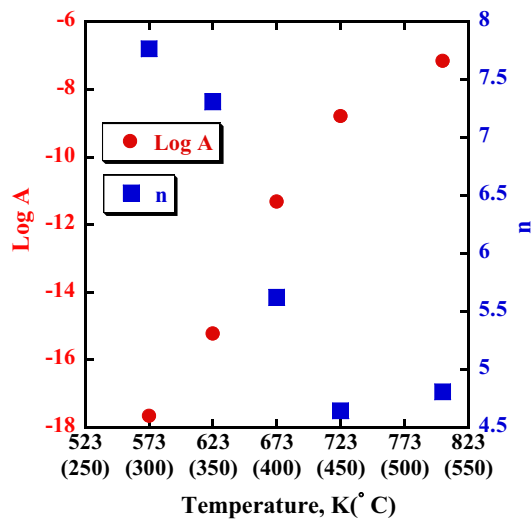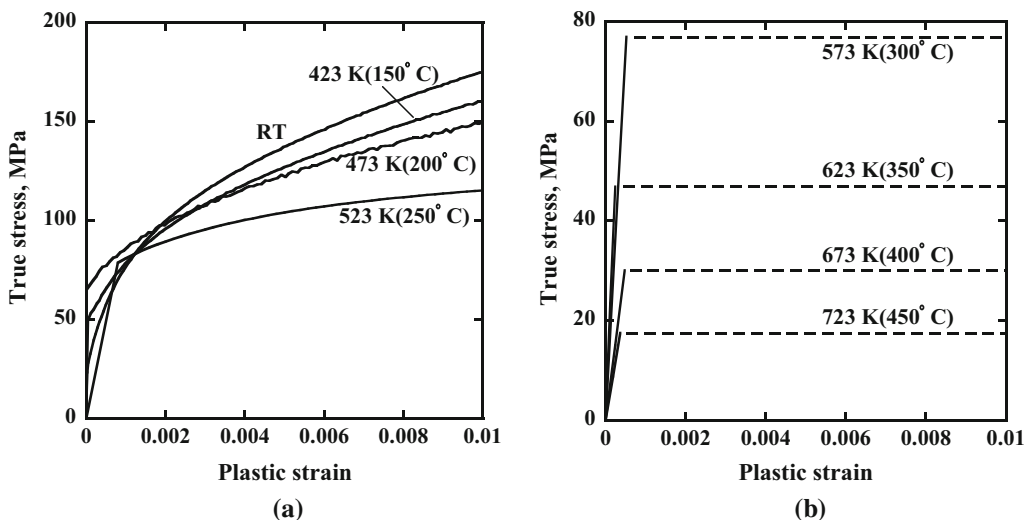

Fig. 9—Inputted creep parameters of ADC12.[6]

Fig. 8—Inputted true stress–plastic strain curves of ADC12: (*a*) RT—523 K (RT—250 °C) and (*b*) 573 K to 723 K (300 °C to 450 °C).[6]
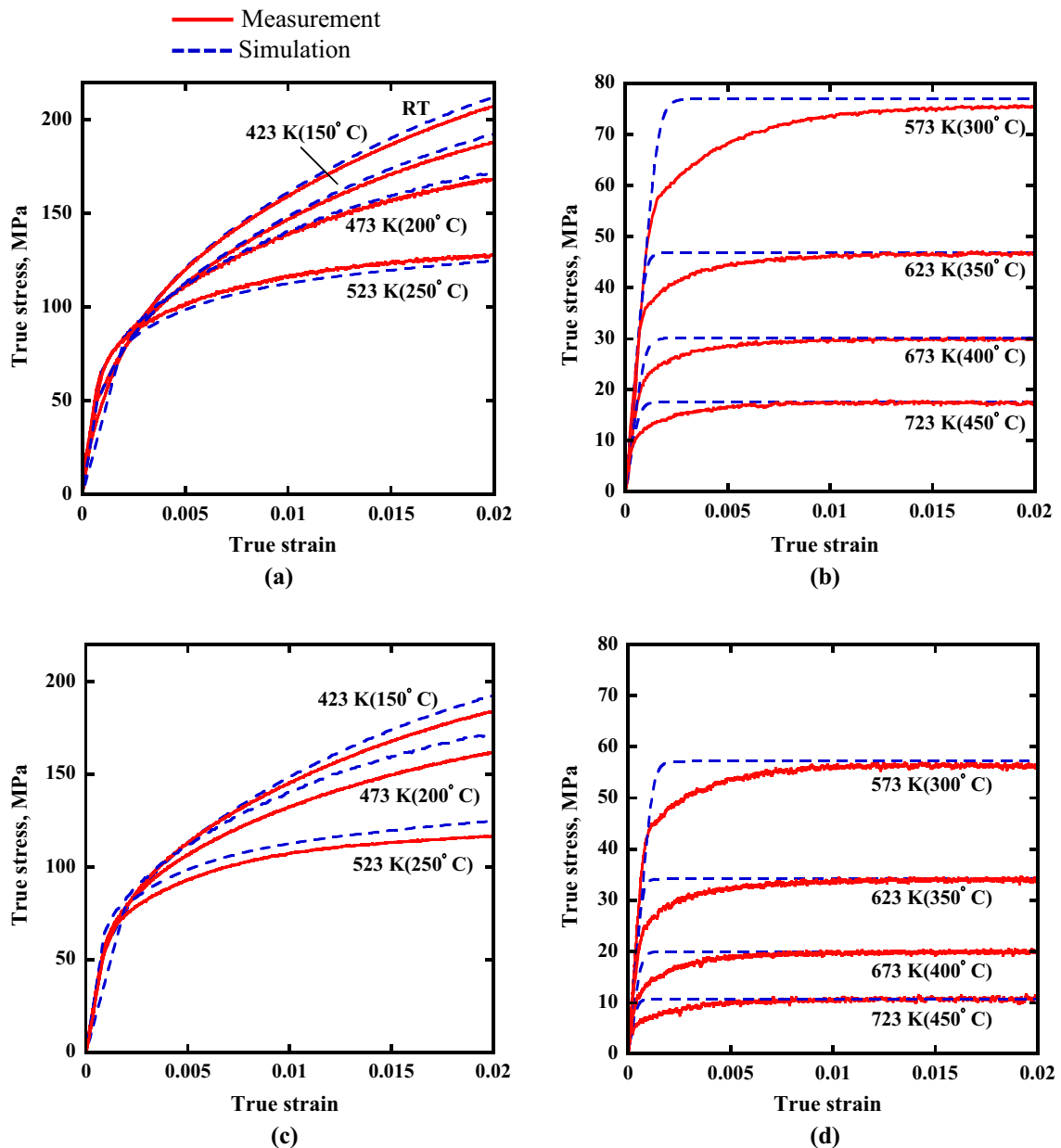
Fig. 10—Measured and predicted stress–strain responses of ADC12 at strain rates of 0.001 s^{-1}: (*a*) RT—523 K (RT—250 °C) and (*b*) 573 K to 723 K (300 °C to 450 °C); and at 0.0001 s^{-1}: (*c*) 423 K to 523 K (150 °C to 250 °C) and (*d*) 573 K to 723 K (300 °C to 450 °C) (Reprinted from Ref. [6]).

machined to test specimens for tensile and the compressive tests. Tensile and compressive tests were conducted at a strain rate of 0.0001 s^{-1} with a high-temperature extensometer. Stress–plastic strain curves of GCI from RT to 873 K (600 °C) were obtained by subtracting the elastic strain component from the stress–strains curve using the Young's moduli, as detailed later. Figure 11 shows the measured and inputted stress–plastic strain curves. The stress–plastic strain curves were inputted as the tabular form for each temperature. The Young's moduli of the GCI were measured using the resonance method. Test samples used for the resonance method were cut from the GCI blocks described above. The measurements were conducted at RT and from 573 K

(300 °C) to 873 K (600 °C) with 100 K steps. The CTE of the GCI was obtained from JMatPro. Figure 12 shows the Young's moduli and CTEs inputted to the cast iron plasticity.

IV. RESULTS AND DISCUSSION

A. *Temperature Histories of the Casting and Liner*

As representative casting temperatures, Figure 13(a) shows measured and simulated temperature histories of the casting at 6 mm distance radially from the liner surface at 45 mm height from the bottom of the liner on the pouring and opposite-pouring sides. Figure 13(b)
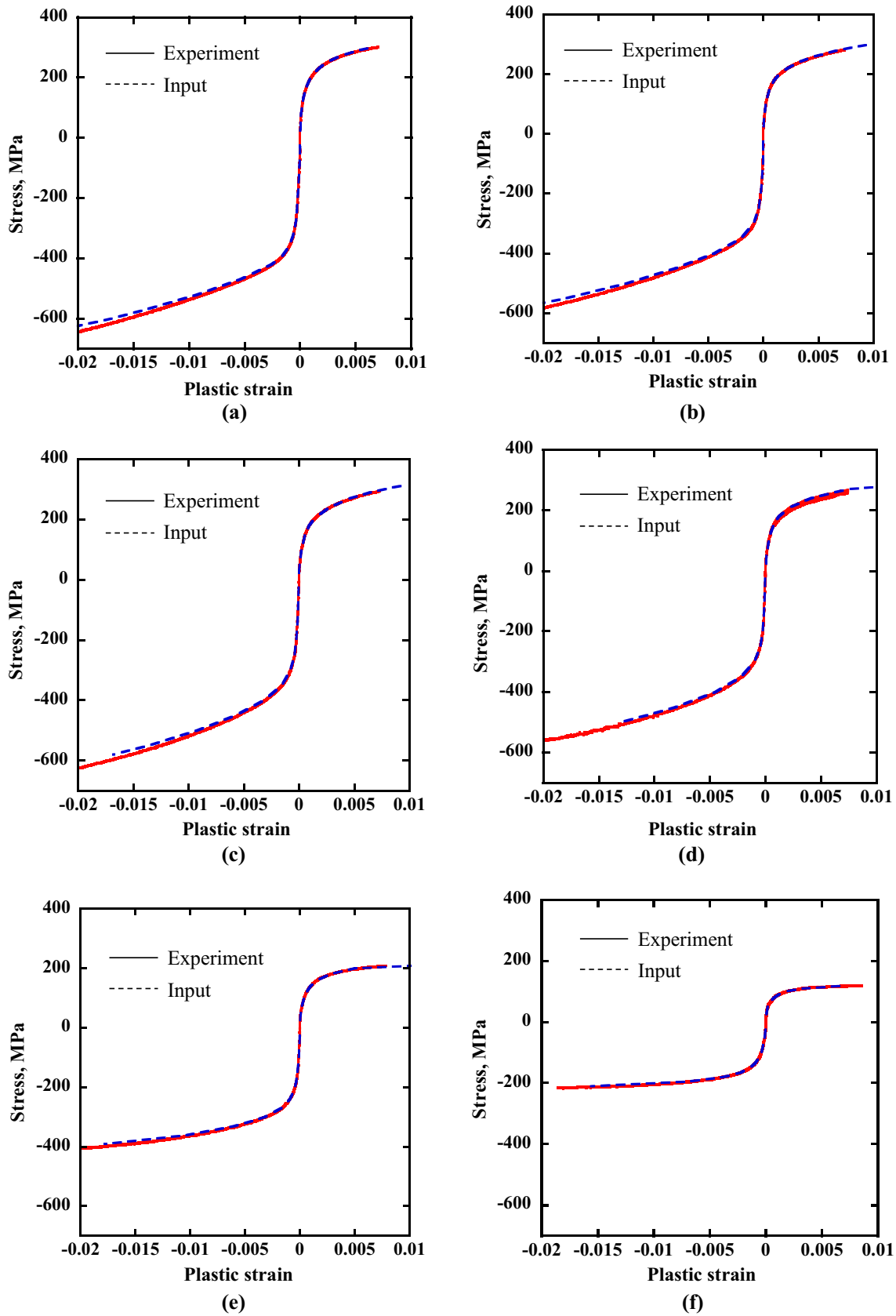
Fig. 11—Stress–plastic strain curves of GCI (ISO 300) at a strain rate of 0.0001 s^{-1} for different temperatures. (*a*) RT, (*b*) 473 K (200 °C), (*c*) 573 K (300 °C), (*d*) 673 K (400 °C), (*e*) 773 K (500 °C), and (*f*) 873 K (600 °C).
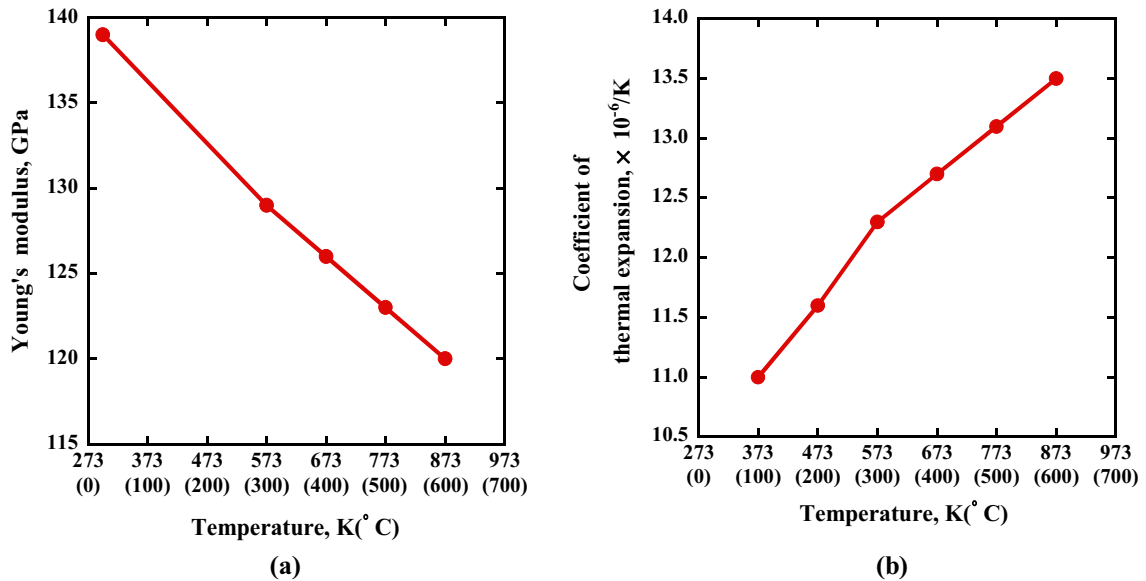
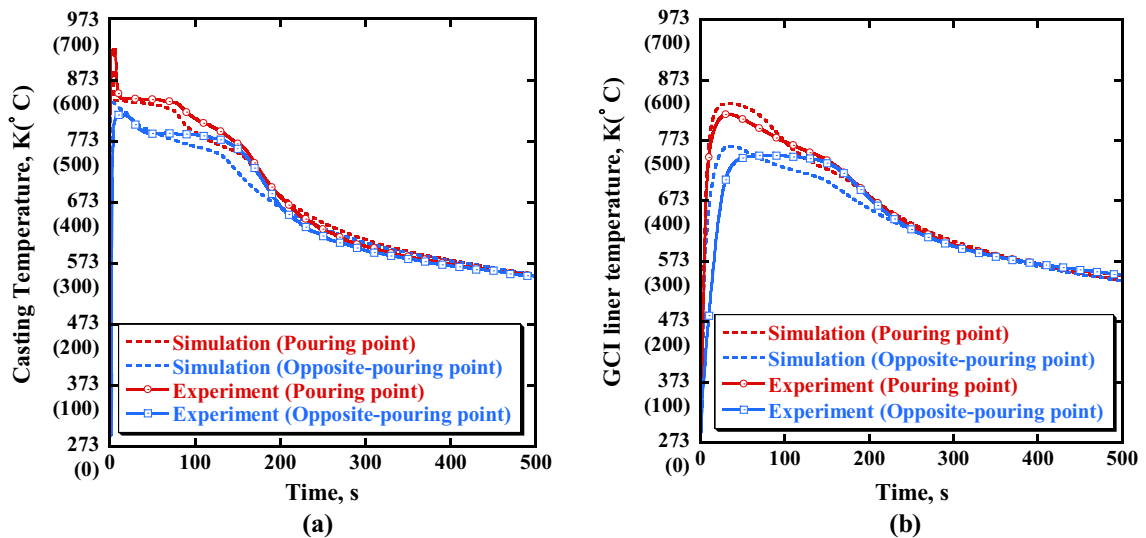Fig. 12—(a) Young's modulus and (b) CTE of GCI inputted to cast iron plasticity.

Fig. 13—Measured and simulated temperature histories of (a) casting and (b) GCI liner.

shows the simulated and experimental temperature histories of the liner on the pouring and opposite-pouring sides at 30 mm height from the bottom of the liner as representative liner temperatures. This study matched the simulated temperature histories of the liner and the casting to the experimental values at all measurement points within 10 pct error during casting. This study applied these results as temperature histories of the casting and the liner for thermal stress analyses.

B. *Residual Stresses of the Casting and the Liner*

Figure 14 shows the measurements of the circumferential residual stresses of the casting and the liner. On casting, there was little difference between the measurement points. The average tensile residual stress was 63.6 MPa. Similar to the casting, the values of the compressive residual stress of the liner at each point were almost equal. The average values were − 202 MPa.

Figure 15 presents a comparison of the average circumferential residual stresses of the casting and the liner between the measurements and simulations. When the classical elastoplastic constitutive equation was used as the casting constitutive equation, the thermal stress analysis, respectively, overestimated the residual stresses of the casting and the liner by 83 and 80 pct. As will be described later, one reason for the overestimation is that the classical constitutive equation is unable to incorporate the recovery. Regarding the elastoplastic-creep constitutive equation, the accuracy of the predicted residual stress of the casting and the liner improved.
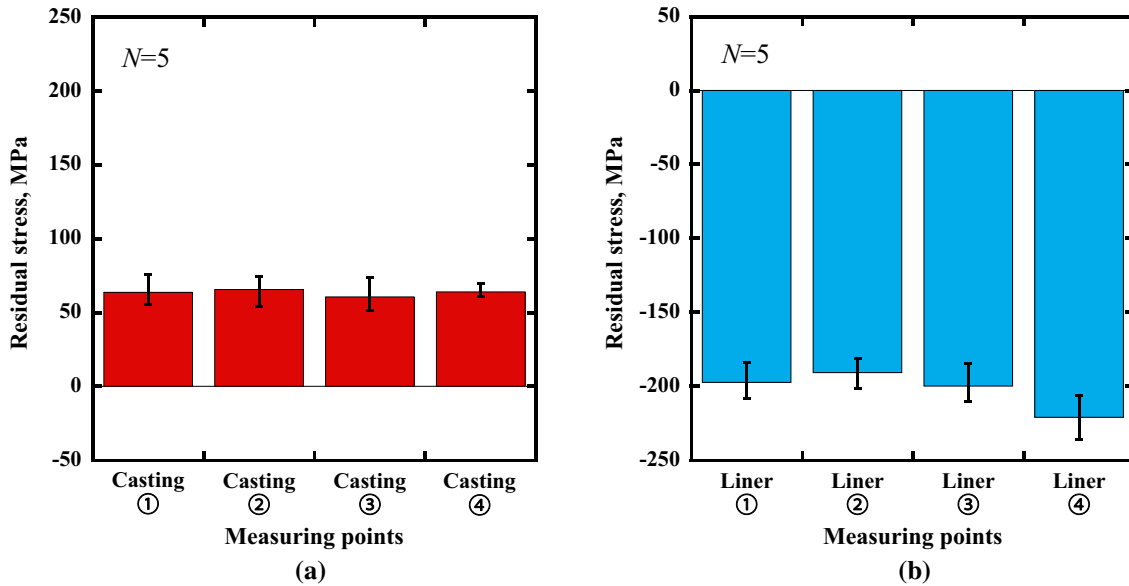
Fig. 14—Measured residual stresses of the circumference direction: (*a*) aluminum casting and (*b*) GCI liner.
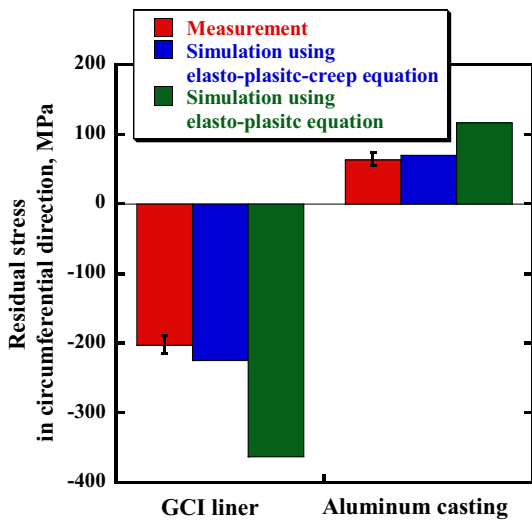

Fig. 15—Comparison of residual stresses in the circumferential direction between measurements, simulation using the elastoplastic-creep model, and simulation using the elastoplastic model.
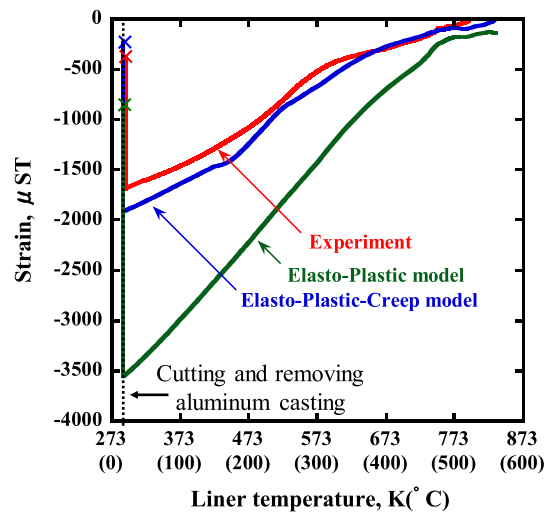

Fig. 16—*In situ* measured circumference direction strain of the GCI liner and simulated values using the elastoplastic model and elastoplastic-creep model.

Figure 16 presents a comparison of the circumferential strain of the liner during cooling between the thermal stress analysis and the measurement. Comparison shows that the simulation using the classical elastoplastic equation overestimated the circumferential strain of the liner during cooling, which indicates that the casting during cooling tightened the liner excessively in the analysis using the classical elastoplastic equation compared with the experiment. Consequently, the overestimated tightening of the aluminum casting induced greater compressive residual plastic strain after removing the aluminum casting in the analysis than in the experiment, as shown in Figure 16. The analysis using elastoplastic-creep equation predicted the development of circumferential strain of the liner during casting more

accurately than the analysis using the classical elastoplastic model. The tightening force of the aluminum casting became weaker in the analysis using the elastoplastic-creep equation than that of the elastoplastic equation. Therefore, the predictive accuracy of the compressive residual plastic strain of the liner after removing the casting improved in the analysis using the elastoplastic-creep equation. This study investigated reasons for improvement of the predictive accuracy of thermal stress analysis using the elastoplastic-creep equation. By investigating the development of strain components of the I-shaped casting during casting, our previous study had already revealed that the predictive accuracy of the residual stress of the casting improved mainly because the alloy constitutive equation incorporated recovery. The present study also specifically
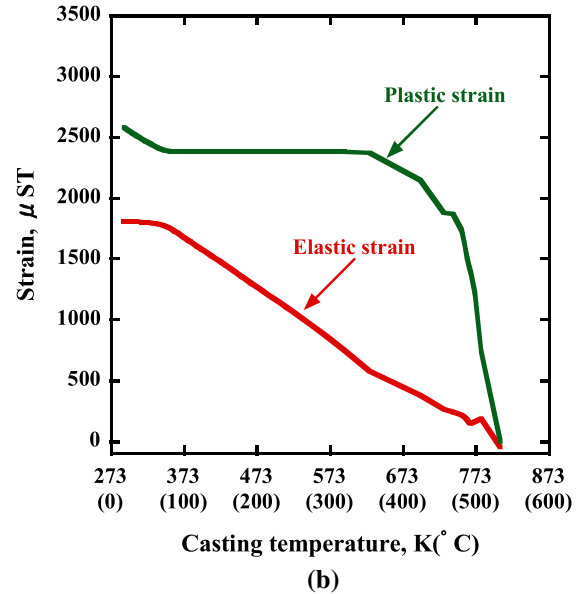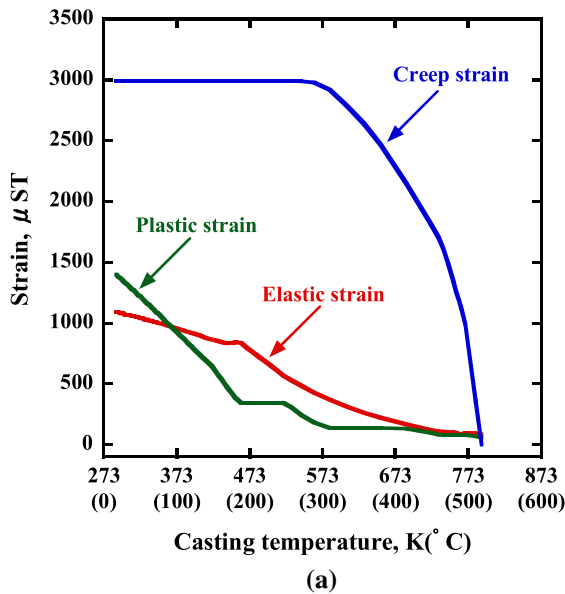
Fig. 17—Development of circumferential strain components of the aluminum casting during casting in the simulation using (*a*) the elastoplastic-creep equation and (*b*) the elastoplastic equation.

examined the development of the simulated strain components of the cylindrical casting during casting.

Figure 17 presents the development of the elastic, plastic, and creep strains of the casting in the circumferential direction. These values were the average of evaluation points shown in Figure 3. The zero-strain point in the figure was assumed as 794 K (521 °C), which was the maximum temperature of the aluminum casting measured in the experiments. Analysis using the classical elastoplastic equation revealed that the yield occurred from 794 K (521 °C), and that the plastic strain developed at temperatures from 794 K (521 °C) to approximately 573 K (300 °C). This result indicates that the equivalent plastic strain accumulated at these temperatures. At temperatures below 573 K (300 °C), the plastic strain did not increase much; the elastic strain developed instead. The strain development behaviors described above indicated that the equivalent plastic strain developed from 794 K (521 °C) to approximately 573 K (300 °C). However, our earlier study revealed that the inelastic (plastic) strain which developed at temperatures higher than 573 K (300 °C) did not contribute to the strain-hardening behavior at RT because of the recovery in ADC12.[14] Therefore, accumulation of the equivalent plastic strain at these temperatures led to the unrealistic increase of the yield stress of the aluminum casting at temperatures below 573 K (300 °C) because the classical elastoplastic equation adopts the equivalent plastic strain as the degree of strain hardening, as shown Eq. [4]. The unrealistic strain hardening of the casting at low temperatures prevented thermal stress developed at low temperatures from being relieved by the occurrence of the plastic strain. This inconvenience led to prediction of the excessive thermal strain during cooling in Figure 16 and to prediction of the excessive residual stress in Figure 15.
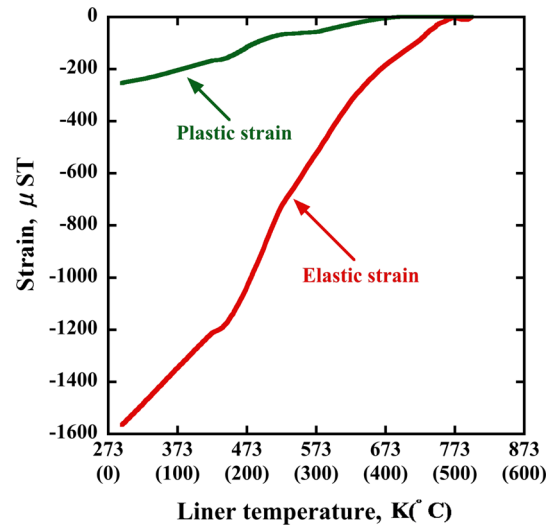

Fig. 18—Development of circumferential stain components of the GCI liner during simulation using the elastoplastic-creep equation for the aluminum casting.

Analysis using the elastoplastic-creep model incorporating recovery showed that almost no plastic strain in the casting developed from 794 K (521 °C) to approximately 573 K (300 °C). Creep strain occurred instead at these temperatures. Therefore, almost no equivalent plastic strain accumulated from 794 K (521 °C) to approximately 573 K (300 °C). When the casting cooled to 573 K (300 °C), less strain hardening of the casting occurred in the analysis using the elastoplastic-creep equation compared to the classical elastoplastic equation calculation. From 573 K (300 °C) or less, the yield occurred, and the plastic strain started to develop, as shown in Figure 17. The occurrence of plastic strain

relaxes the thermal stress developed at low temperature, unlike the strain-hardened casting in the simulation using the elastoplastic equation. Therefore, less strain hardening of the casting led to less tightening of the aluminum casting to the liner compared to that implied by the classical elastoplastic equation results. Less hardening led to improved accuracy of the circumferential strain prediction in Figure 16 and accuracy of the residual stress in Figure 15.

Figure 18 presents development of circumferential strain components of the GCI liner in the simulation using the elastoplastic-creep equation in Figure 16. Tightening of the liner induced the yield of the GCI liner from approximately 673 K (400 °C). The compressive plastic strain developed from approximately 673 K (400 °C) to 298 K (25 °C). The final residual plastic strain in Figure 18 corresponds to the residual strain of the GCI liner in the simulation using elastoplastic-creep equation after removing the aluminum casting in Figure 16.

Figure 19 presents a comparison of the simulated and measured distortions of the liner at RT. The liner characteristics obtained from the analysis using elastoplastic equation implied excessive distortion, in contrast to the experiment result. The analysis using the elastoplastic-creep equation predicted the distortion more accurately because the simulated tightening by the aluminum casting became weaker than elastoplastic model.

From the discussion presented above, this study has demonstrated that the recovery behavior is a key factor to be considered in the alloy constitutive equation to predict residual stress and deformation of a cylindrical aluminum casting with a GCI liner, as with an I-shaped casting. However, even with the elastoplastic-creep constitutive equation considering the recovery, the residual stress of the GCI liner and the aluminum casting and the deformation amount of the liner were still calculated somewhat excessively. This trend was the same as that found for the simple I-shaped casting used for validating our elastoplastic-creep equation in our previous study.[7] The elastoplastic-creep equation used for the present study excessively reproduces the initial strain-hardening transient region of stress–strain curves at the high-temperature range while exhibiting good agreement in the steady-state flow stress region between the simulation and experiment, as shown in Figure 10. Furthermore, in our constitutive equation, the recovery behavior is reproduced conveniently by treating the strain generated in the steady stress state at high temperatures as the creep strain. Therefore, it appears possible to improve the prediction accuracy by using a constitutive formula that can reproduce the stress–strain curve and the recovery behavior more accurately.

V. CONCLUSION

The thermal stress of a cylindrical aluminum casting with a GCI liner was simulated using classical elastoplastic and the elastoplastic-creep constitutive equations. The former was unable to represent the recovery and the strain-rate dependence of the stress–strain curve, but the latter was able to do so. Comparisons between the simulations and the measurements were conducted for the residual stress of the aluminum casting and the GCI liner, the GCI liner deformation, and *in-situ* measurements of the strain that developed in the liner during casting. From those comparisons, this study conferred the following additional knowledge:

(1) Thermal stress calculation using the classical elastoplastic model overestimated the circumferential compressive strain of the GCI liner from 794 K (521 °C) to RT. The calculated residual stresses of the casting and the liner were 83 and 80 pct excess, respectively, compared with the experiments. Because it indicates excessive tightening by the aluminum casting, results of simulations relying on that model implied the more excessive distortion of the GCI liner than that found through experimentation.

(2) Use of the elastoplastic-creep constitutive equation improved the predictive accuracy of *in-situ* measurements of the circumferential strain of the liner during casting. The simulated residual stresses of the aluminum casting and the GCI liner showed good agreement with the experimentally obtained results. The corresponding errors were predicted with 10 and 11 pct errors, respectively. The resultant distortion of the GCI liner was simulated more accurately than when using the elastoplastic equation.

(3) The development of each strain component of the aluminum casting during cooling was investigated to ascertain the reason for the improved predictive accuracy of the residual stress and deformation. Results showed incorporation of recovery in the elastoplastic-creep constitutive equation as the main reason for the improvement of the predictive accuracy for thermal stress analysis of the aluminum cylindrical casting with a GCI liner.
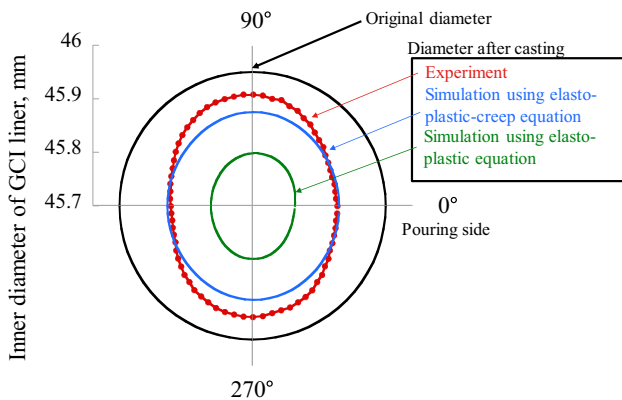
Fig. 19—Comparison of the diameter changes of GCI liner before and after casting between experiments, simulation using elastoplastic-creep equation, and simulation using elastoplastic equation.

REFERENCES

1. E. Carrera, A. Rodriguez, J. Talamantes, S. Valtierra, and R. Colas: *J. Mater. Process. Tech.*, 2007, vol. 189, pp. 206–10.
2. A. Lombardi, F. D'Elia, C. Ravindran, D. Sediako, B.S. Murty, and R. MacKay: *Metall. Mater. Trans. A*, 2012, vol. 43A, pp. 5258–70.
3. A. Lombardi, D. Sediako, C. Ravindran, and R. MacKay: *SAE Int. J. Mater. Manf.*, 2014, vol. 7, pp. 415–20.
4. Ahmad, S., Sediako, D., Lombardi, A., Ravindran, C., MacKay, and R., Nabawy, A.: *SAE Technical Papers* 2016.
5. P. Hofer, E. Kaschnitz, and P. Schumacher: *JOM*, 2014, vol. 66, pp. 1638–46.
6. Y. Motoyama, H. Shiga, T. Sato, H. Kambe, and M. Yoshida: *Metall. Mater. Trans. A*, 2016, vol. 47A, pp. 5598–5608.
7. Y. Motoyama, H. Shiga, T. Sato, H. Kambe, and M. Yoshida: *Metall. Mater. Trans. A*, 2017, vol. 48A, pp. 2960–70.
8. S. Dong, Y. Iwata, Y. Sugiyama, and H. Iwahori: *Mater. Trans.*, 2010, vol. 51, pp. 371–76.
9. U. Wasmuth, L. Meier, M. Hofmann, M. Mühlbauer, V. Stege, and H. Hoffmann: *CIRP Ann. – Manuf. Technol.*, 2008, vol. 57, pp. 579–82.
10. J. Čech, K. Palán, R. Zalaba, K. Švaříček, and D. Bařinová: *Archiv. Foundry*, 2004, vol. 4, pp. 93–103.
11. Abaqus 6.10 theory manual 4.3.7, pp. 1–8.
12. H. Shiga, T. Satoh, H. Kambe, Y. Motoyama, and M. Yoshida: *J. JFS*, 2015, vol. 87 (7), pp. 453–59.
13. K. Shinji, H. Takahashi, Y. Motoyama, and M. Yoshida: *J. Jpn. Inst. Light Met.*, 2013, vol. 63, pp. 253–59.
14. Y. Motoyama, G. Saito, H. Ono, and M. Yoshida: *Mater. Sci. Eng. A*, 2017, vol. 684, pp. 660–67.